Available online at www.sciencedirect.com
ScienceDirect
International Journal of Thermal Sciences 47 (2008) 1676–1687
International Journal of Thermal Sciences
www.elsevier.com/locate/ijts

Molten salt mixture properties in RELAP5 code for thermodynamic solar applications

Roberta Ferri [a,*], Antonio Cammi [b], Domenico Mazzei [c]

[a] *SIET S.p.A. Via Nino Bixio 27, 29100 Piacenza, Italy*
[b] *Politecnico di Milano, CESNEF Via Ponzio 34/3, 20133 Milano, Italy*
[c] *ENEA Via Anguillarese 301, 00123 S. Maria di Galeria, Roma, Italy*

Received 18 May 2007; received in revised form 10 January 2008; accepted 20 January 2008

Available online 14 February 2008

Abstract

Ongoing research on innovative and environmentally sustainable systems for energy production, as an alternative to the traditional sources, led ENEA to investigate high temperature heat generation by solar power and the subsequent energy collection and storage. An experimental facility, the Prova Collettori Solari (PCS), was built at the ENEA Casaccia Research Centre to test the most innovative components before industrialization and to determine the effectiveness of the foreseen thermodynamic cycle utilizing a molten salt mixture, heated in a solar collector irradiated by parabolic mirrors. In parallel with the experimental investigation, the development of a numerical tool for thermal-fluid-dynamic simulation of circuits, with such a mixture as the primary heat transfer fluid, was pursued and the RELAP5 code was modified accordingly. Thermo-physical property tables were developed for the liquid and steam phases of the molten salt mixture and inserted into the RELAP5 code. The modified code was benchmarked versus experimental data. The entire PCS facility was then simulated with various operational transients aimed at studying both the dynamic and thermal behavior of the whole system.

This paper summarizes the choices and assumptions for the property definition of the molten salts, their introduction in the RELAP5 code, and the main results of the operational transients simulation in the PCS facility.

Keywords: RELAP5; Molten salts; Thermodynamic solar application; Parabolic mirrors; High temperature heat generation

1. Introduction

The production of electric energy by renewable sources as an alternative to or integrated with the traditional fossil fuel combustion is a more desirable objective of developed countries energy policies. The use of molten salts as storage medium and heat transfer fluid was proposed and tested as an alternative to the poor environmentally compatible mineral oil, traditionally used in solar power plants [1,2]. Within the framework of a research and development (R&D) activity on solar applications for electric energy and hydrogen production, ENEA developed a system for high temperature heat generation by joining already existing solar technologies with innovative components. In particular, parabolic linear mirrors were developed that direct incident solar radiation to a collector to heat up a molten salt fluid mixture of 60% $NaNO_3$ and 40% KNO_3 by weight to 550 °C and collect the mixture in a storage tank to delay its heat release to night or cloudy periods. A scheme for a concentration type solar plant for energy production is shown in Fig. 1 [3]. However, the industrialization of the new components and systems would be possible only after a period of experimentation. To this end, the Prova Collettori Solari (PCS) facility was built at the ENEA Casaccia laboratories to investigate all aspects of new technology development, mostly within sight of a large-scale prototype plant.

In support of design and testing, the need for a numerical tool emerged, that would be suitable to simulate hydraulic circuits containing the chosen molten salt mixture both in steady state and transient conditions. The RELAP5 best estimate code was identified as a possible powerful means for such a goal,

* Corresponding author. Fax: +39 0523 329010.
E-mail addresses: ferri@siet.it (R. Ferri), antonio.cammi@polimi.it (A. Cammi), mazzei@casaccia.enea.it (D. Mazzei).

1290-0729/$ – see front matter
doi:10.1016/j.ijthermalsci.2008.01.007

Nomenclature

ENEA	Ente per le Nuove tecnologie, l'Energia e l'Ambiente
PID	Proportional Integral Derivative
PCS	Prova Collettori Solari
RELAP	REactor Loss of coolant Analysis Program
R&D	Research and Development
SIET	Società Informazioni Esperienze Termoidrauliche
tmdpvol	time dependent volume (RELAP component)
c_p	specific heat capacity ..... $J\,kg^{-1}\,K^{-1}$
k	isothermal compression coefficient ..... Pa^{-1}
K	thermal conductivity ..... $W\,m^{-1}\,K^{-1}$
h	specific enthalpy ..... $J\,kg^{-1}$
P	pressure ..... Pa
s	specific entropy ..... $J\,kg^{-1}\,K^{-1}$
T	temperature ..... K
u	specific internal energy ..... $J\,kg^{-1}$
v	specific volume ..... $m^3\,kg^{-1}$

Greek symbols

β	isobaric expansion coefficient ..... K^{-1}
μ	dynamic viscosity ..... Pa s
σ	steam surface tension ..... $N\,m^{-1}$

Subscripts

crit	critical point
gl	vaporization
l	liquid
s	steam
sat	saturation
trip	triple point

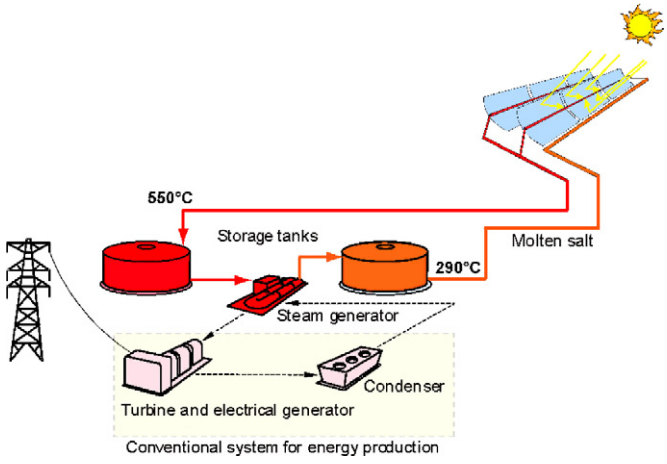

Fig. 1. Scheme of a concentration type solar plant for energy production.

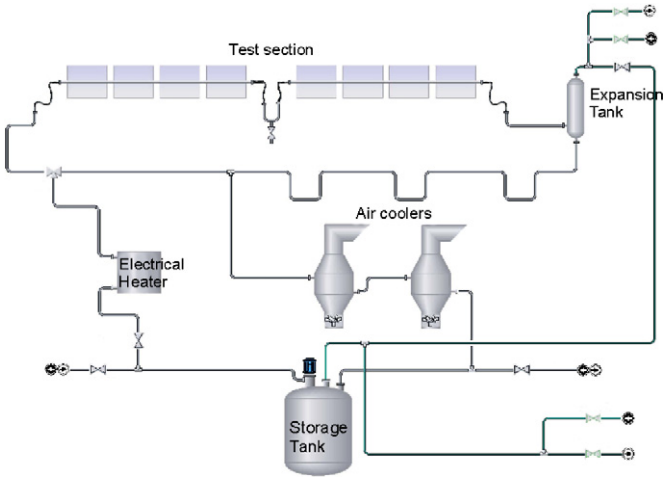

Fig. 2. Scheme of the PCS facility.

having been a code developed for water cooled nuclear reactors and later applied to fusion and molten metal nuclear power plants. The RELAP5 code is based on nonhomogeneous and nonequilibrium model for the two-phase systems that is solved by a fast, partially implicit numerical scheme to permit economical calculations of system transients [4]. The use of the RELAP5 code with fluids different from light and heavy water was possible by specific subroutine modification and the introduction of proper thermo-physical property tables for each fluid. The molten salt mixture tables were developed, introduced in the code and tested by the SIET company and Politecnico di Milano in order to verify the effectiveness and reliability of the new tool suitable to predict experimental data and to investigate full-scale plant behavior.

2. The PCS facility description and operation

A scheme of the PCS facility is shown in Fig. 2. It consists of a full-scale experimental circuit suitable to test the entire solar radiation collection system during conditions as close as possible to the real conditions. Prototypes of the linear parabolic collectors, the receiver collectors, and the molten salt mixture fluid are tested together with other possible critical components of the electrical energy production system. The test section consists of the parabolic mirrors and the receiver collector. A storage tank, a circulation pump, an electric heater, an expansion tank, a heat exchanger, and connecting piping constitute the rest of the circuit. An additional tank, not shown in the picture, is available for melting the salt and charge–discharge of the circuit.

Two parabolic linear collectors, east–west oriented, 6 m wide and 50 m long, are equipped with a computer regulated hydraulic actuation system; their position is adjusted based on time of the day and day of the year.

During normal operation, fluid is circulated in the circuit by a vertical centrifugal pump immersed in the storage tank whose speed can be regulated by an inverter. The nominal mass flow rate is 6 kg/s. The electric heater regulates the fluid temperature at the test section inlet on the basis of the specified test. While crossing the collector, the working fluid heats up by receiving the solar energy concentrated by the mirrors;

Table 1
Main characteristics of the PCS facility

Parameter	Value	Units
Number of parabolic collectors east–west oriented	2	–
Active length of each collector	48	m
Active surface of each collector	553	m^2
Minimum temperature of fluid	290	°C
Maximum temperature of fluid	550	°C
Peak power	393	kW

it cools down by crossing two air coolers. Being an experimental facility, the heat collected is dissipated into the atmosphere. The airflow can be regulated by electric fans to obtain the specified fluid temperature in the storage tank and consequently at the test section inlet. The air-salt heat exchangers in the two cooler units in series consist of finned tubes of the same diameter and thickness as the main piping. The main characteristics of the PCS facility are summarized in Table 1.

3. Molten salt mixture thermo-physical properties and their introduction into the RELAP5 code

The reference salt mixture weight proportions are: 60% $NaNO_3$ and 40% KNO_3.

The correlations describing both the liquid and steam phase physical properties for all RELAP5 fluids are entered in subroutines in the code.

ENEA used the liquid phase experimental property correlations [5] that were already determined by Sandia National Laboratory [6]. However, no correlation was available from the literature or experimental data for the steam phase. The steam phase properties were determined based on physical laws, assumptions, and tuning cases. In order to run properly, the RELAP5 code requires the liquid and steam state of a fluid to be completely described by correlations, regardless of whether the application is utilized exclusively in the subcooled liquid phase. For the PCS application, the steam phase is needed only for partial pressure balance of the partially filled storage tanks. Thus, the molten salt mixture steam quantity is negligible and the approximations on the saturation curve and steam phase correlations are assumed to be acceptable, because the PCS is operated in conditions far from the saturation.

All correlations implemented in the code are reported below.

3.1. The liquid state

The molten salt mixture can be used between 533 and 873 K, covering the PCS temperature of interest range. With decreasing temperature, the mixture begins to crystallize at 511 K and is completely solid at 494 K. The last value has been assumed as the minimum temperature in the fluid property tables.

The molar mass of $NaNO_3$ is 84.995 kg/kmol, of KNO_3 is 101.1033 kg/kmol, and of the mixture is 91.438 kg/kmol.

The liquid specific volume versus temperature is given by:

$$v_l = \frac{1}{2090 - 0.636 \bullet (T - 273.15)} \quad (\mathrm{m^3/kg}) \quad (\text{Temperature in K}) \tag{1}$$

The liquid specific heat versus temperature is given by:

$$c_{pl} = 1443 + 0.172 \bullet (T - 273.15) \quad [\mathrm{J/(kg\,K)}] \tag{2}$$

The liquid dynamic viscosity versus temperature is given by:

$$\mu_l = \frac{22.714 - 0.12 \bullet (T - 273.15) + 2.281 \bullet 10^{-4} \bullet (T - 273.15)^2}{1000} - \frac{1.474 \bullet 10^{-7} \bullet (T - 273.15)^3}{1000} \quad (\mathrm{Pa\,s}) \tag{3}$$

The liquid thermal conductivity is given by:

$$K_l = 0.443 + 1.9 \bullet 10^{-4} \bullet (T - 273.15) \quad [\mathrm{W/(m\,K)}] \tag{4}$$

The liquid specific internal energy is given by:

$$u_l = 0.086 \bullet T^2 + 1396.0182 \bullet T - \frac{P}{[2090 - 0.636 \bullet (T - 273.15)]} \quad (\mathrm{J/kg}) \tag{5}$$

being:

$$u_l = h_l - P \bullet v_l = \int c_{pl}\,\mathrm{d}T - P \bullet v_l \tag{6}$$

with h_l liquid specific enthalpy.

The liquid entropy is given by:

$$s_l = \int \frac{c_{pl}}{T}\,\mathrm{d}T = 1396.0182 \bullet \ln(T) + 0.172 \bullet T \quad [\mathrm{J/(kg\,K)}] \tag{7}$$

The liquid isobaric expansion coefficient is given by:

$$\beta_l = \frac{1}{v_l}\left(\frac{\partial v_l}{\partial T}\right)_p = \frac{0.636}{2263.72 - 0.636 \bullet T} \quad (\mathrm{K^{-1}}) \tag{8}$$

The general expression for the isothermal compression coefficient is:

$$k_l = -\frac{1}{v_l}\left(\frac{\partial v_l}{\partial P}\right)_T \quad (\mathrm{Pa^{-1}}) \tag{9}$$

A correlation of specific volume versus pressure was not available, therefore, it was not possible to obtain the isothermal compression coefficient by the above expression. Thus, the following correlation as a function of temperature typical of liquid metals was found in the literature and used in the computer code:

$$k_l = k_0 \bullet e^{b(T - T_0)} = 3.97 \bullet 10^{-11} \bullet e^{[1.37 \bullet 10^{-3} \bullet (T - 293.15)]} \quad (\mathrm{Pa^{-1}}) \tag{10}$$

Because the values of the liquid isothermal compression coefficient are very small (on the order of 10^{-10} $\mathrm{Pa^{-1}}$), the utilization of coefficients k_0 and b related to mercury was considered as an acceptable approximation [7,8].

3.2. The steam state

Because the salt mixture experimental correlations for the steam state within the working pressure and temperature ranges are not available, the perfect gas law validity hypothesis was used.

The saturation curve is described by the Clausius–Clapeyron correlation:

$$P = e^{(B-\frac{A}{T})} \quad [9\text{–}11] \tag{11}$$

The coefficients A and B were obtained by assumptions and imposed conditions that, even if different from reality, were suitable to satisfy the continuity between liquid and steam at the critical point. The following conditions were assumed that in a three equation system provide the appropriate A, B and T_{crit} (critical point temperature):

(1) Saturation temperature at 0.1 MPa equal to 894 K [12];
(2) Critical point pressure $P_{\text{crit}} = 10$ MPa (assumed value, because it is not known);
(3) Liquid specific volume equal to steam specific volume at the critical point ($v_{l\text{crit}} = v_{s\text{crit}}$).

The subsequent saturation curves of pressure and temperature are:

$$P_{\text{sat}} = e^{(17.69185-\frac{5523.9586}{T})} \tag{12}$$

$$T_{\text{sat}} = \frac{5523.9586}{17.69185 - \ln(P)} \tag{13}$$

The critical point temperature, $T_{\text{crit}} = 3510.05$ K, and the specific volume, $v_{\text{crit}} = 0.031917\ \text{m}^3/\text{kg}$.

The triple point, which represents the minimum limit of liquid existence, is determined to be $T_{\text{trip}} = 494$ K; $P_{\text{trip}} = 671.6568$ Pa; and $v_{\text{trip}} = 5.1294$ E–4 m^3/kg.

Using the ideal gas law, the steam specific volume is given by:

$$v_s = \frac{8.314 \bullet 1000}{91.438} \bullet \frac{T}{P} \quad (\text{m}^3/\text{kg}) \tag{14}$$

The correlation for the specific heat of vaporization is:

$$h_{\text{gl}} = (0.0507) \bullet (10^7 - P) \quad (\text{J/kg}) \tag{15}$$

Because this quantity was unavailable from experimental data, it was obtained by combining the Clausius–Clapeyron correlation in derivative form, the ideal gas law, and the saturation curve, and using the same trend for specific heat of vaporization versus pressure of water [13].

The steam specific heat correlation, based on the ideal gas behavior, is:

$$c_{ps} = (100 + T) \bullet \frac{1000}{91.438} \quad [\text{J/(kg K)}] \tag{16}$$

The coefficients in brackets were determined based on a series of iterative numerical calculations until no numerical error occurred.

The steam specific internal energy correlation is given by:

$$\begin{aligned} u_s = {} & 0.086 \bullet \left(\frac{5523.9586}{17.69185 - \ln(P)}\right)^2 \\ & + 1396.0182 \bullet \left(\frac{5523.9586}{17.69185 - \ln(P)}\right) \\ & + (0.0507) \bullet (10^7 - P) \\ & + (100 + T) \bullet \frac{1000}{91.438} \bullet \left(T - \frac{5523.9586}{17.69185 - \ln(P)}\right) \\ & - 90.92 \bullet T \quad (\text{J/kg}) \end{aligned} \tag{17}$$

where:

$$u_s = h_s - P v_s = h_{l\text{sat}} + h_{\text{gl}} + \int_{T_{\text{sat}}}^{T} c_{ps}\, \text{d}T - P v_s \tag{18}$$

Based on a series of numerical calculations, an average value of c_{ps} was determined and the above formula was modified to:

$$u_s = h_s - P v_s = h_{l\text{sat}} + h_{\text{gl}} + c_{ps} \bullet (T - T_{\text{sat}}) - P v_s \tag{19}$$

The steam specific entropy correlation [J/(kg K)] is given by:

$$\begin{aligned} s_s = {} & 1396.0182 \bullet \ln\left(\frac{5523.9586}{17.69185 - \ln(P)}\right) \\ & + 0.172 \bullet \left(\frac{5523.9586}{17.69185 - \ln(P)}\right) \\ & + \frac{(0.0507) \bullet (10^7 - P)}{(\frac{5523.9586}{17.69185 - \ln(P)})} \\ & + (100 + T) \bullet \frac{1000}{91.438} \bullet \ln \frac{T}{(\frac{5523.9586}{17.69185 - \ln(P)})} \quad [\text{J/(kg K)}] \end{aligned} \tag{20}$$

where:

$$S_v = S_{l\text{sat}} + \frac{h_{\text{gl}}}{T_{\text{sat}}} + \int_{T\text{sat}}^{T} C_{ps} \frac{\text{d}T}{T} \tag{21}$$

As for U_s, an average value of c_{ps} was used and the above formula was modified to:

$$s_v = s_{l\text{sat}} + \frac{h_{\text{gl}}}{T_{\text{sat}}} + c_{ps} \bullet \ln\left(\frac{T}{T_{\text{sat}}}\right) \tag{22}$$

The steam isobaric expansion coefficient (ideal gas) is given by:

$$\beta_s = \frac{1}{T} \quad (\text{K}^{-1}) \tag{23}$$

The steam isothermal compression coefficient (ideal gas) is given by:

$$k_s = \frac{1}{P} \quad (\text{Pa}^{-1}) \tag{24}$$

The steam dynamic viscosity versus temperature is given by:

$$\mu_s = 6 \bullet 10^{-6} \bullet e^{(0.0046 \bullet T)} \quad (\text{Pa s}) \tag{25}$$

Because an effective trend is not available from experimental data, the above correlation was obtained by multiplying the molten salt liquid viscosity by the steam/water viscosity ratio as a function of temperature and then interpolating the points.

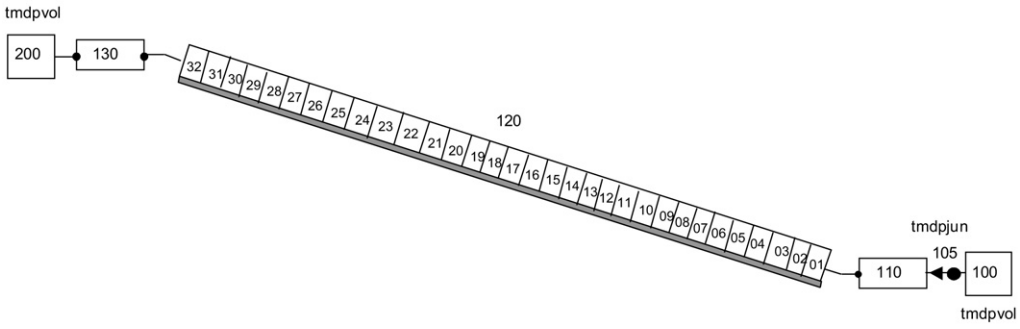

Fig. 3. Nodalization of the PCS electric heater.

Table 2
Experimental and calculated quantities on the PCS electric heater

Parameter	Units	Experimental value	Measurement uncertainty	Calculated value	Calculated-difference
Heater inlet fluid temperature	K	597.05	±1.10	597.17	0.12
Heater outlet fluid temperature	K	619.05	±1.10	620.14	1.09
Wall temperature at half of heater length	K	641.45	±1.10	641.64	0.19
Wall temperature at full heater length	K	644.95	±1.10	644.97	0.02
Heater inlet absolute pressure	kPa	374.91	±2.20	377.13	2.22
Heater outlet absolute pressure	kPa	334.33	±2.20	332.74	−1.59
Heater electrical power	kW	217.7	±2.30	217.7*	0
Fluid mass flow rate (OF)	kg/s	6.19	±0.06	6.19*	0
Fluid mass flow rate (UF)	kg/s	6.55	±0.06	6.19*	0.36
Fluid thermal power	kW	218.59	±7.5	213.5	−5.09
Heater inlet/outlet differential pressure	kPa	42	±3.1	44.39	2.39

* Value assumed in the calculation.

An analogous choice was made for the steam thermal conductivity. The ensuing correlation is:

$$K_s = 0.0009 \bullet e^{(0.0048 \bullet T)} \quad [\mathrm{W/(m\,K)}] \tag{26}$$

The steam surface tension is also not known. Therefore, the lead related correlation was inserted into the code:

$$\sigma = 458 \bullet 10^{-3} - 0.13 \bullet 10^{-3} \bullet (T - 600.55) \quad (\mathrm{N\,m^{-1}}) \tag{27}$$

In addition to the above described correlations implemented in the code, a further modification that inhibited the salt mixture steam condensation on the walls was needed to avoid premature stopping of the computer code run, because such condensation is negligible in single phase system cases for which this numerical tool was developed.

4. Molten salt property tables validation versus experimental data

After the code modification, a comprehensive assessment and validation of the new fluid property tables were performed on the basis of experimental data recorded on the PCS facility electric heater. The physical correlations introduced into the code were verified along with their numerical stability.

The PCS electric heater consists of an AISI 316 stainless steel coil pipe of 54.76 mm inner diameter and 2.77 mm thickness. This once-through heat exchanger is directly heated by the Joule effect (nominal voltage 60 V), shaped in eight 1.31 m average diameter coils with 2 × D pitch, and being thermally insulated.

Some fundamental experimental measures were selected [14] and a numerical model of the test section was developed, Fig. 3. The correspondence between experimental and calculated data was verified by ensuring that the calculated values were within the measurement uncertainty of the corresponding experimental values.

Table 2 reports the variables selected for the validation process, their experimental values recorded at the electric heater nominal test conditions, their measurement uncertainty calculated as described above, the values of the same parameters predicted by the code and their difference with respect to the experimental values. In almost all cases the above assumed validation criterion was verified and the calculated values were within the experimental uncertainty. In a few cases the calculated values were not within the experimental uncertainty, but their use can be justified by the numerical model set-up choices and imposition of boundary conditions. In particular, two different values of measured mass flow rates were available as well as two values of power. Mass flow rate measured by the orifice was assumed in the model as well as the heater electrical power. This resulted in these parameters being outside of the established boundary. Regardless, given the good agreement between all the other parameters, the validation criterion was considered satisfied and the new modified version of RELAP5 was declared suitable for system transient simulation in the PCS operating range.

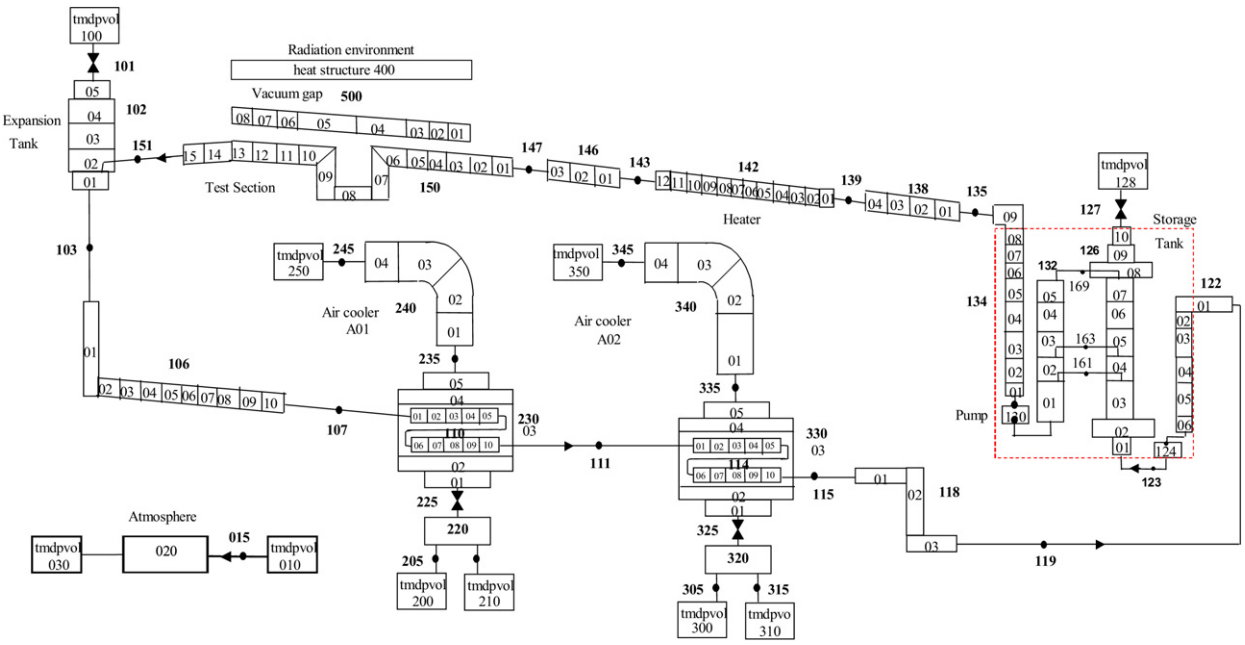

Fig. 4. Nodalization of the PCS facility.

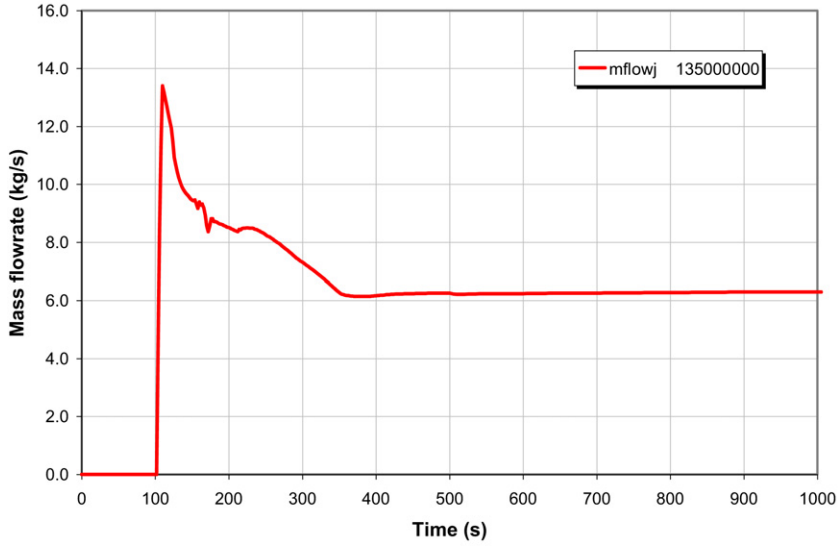

Fig. 5. Transient No. 1: Pump mass flow rate (the initial phase).

5. PCS facility numerical simulation

A complete nodalization of the PCS facility was created by reproducing the hydraulic circuit and all components on the basis of constructive drawings, geometry and material characteristics [15]. The PCS nodalization is shown in Fig. 4. Pressure loss coefficients were determined based on geometrical singularity type and experimental data. The effective pump characteristics were loaded in the code in the form of homologous curves. The storage tank was simulated with parallel channels with transversal junctions in order to avoid thermal stratification due to the one-dimensionality of the code. The expansion tank was simulated as a single channel, because of its small dimensions and the low influence of stratification on the thermal inertia of the system.

The vacuum gap around the test section, that thermally separates the collector from the atmosphere, was simulated by imposing a very low pressure (1 Pa) in the related pipe. Power to the test section was provided by a thermal structure as though the power were directly generated within it, while the radiation heat structure was simulated representing the atmosphere. The radiant emittances of all test section materials were also input.

The air coolers, air side, were simulated from the geometrical and fluid dynamic point of view and both the natural and forced air circulation were provided by means of gates that opened when the salt temperature at the second air cooler outlet reached ($T_{\text{set point}} - 5$ K). The air fans actuated when the salt temperature at the second air cooler outlet was ($T_{\text{set point}} + 2$ K). Moreover a proportional integral derivative (PID) controller regulated the air flow at the first air cooler and simply on/off

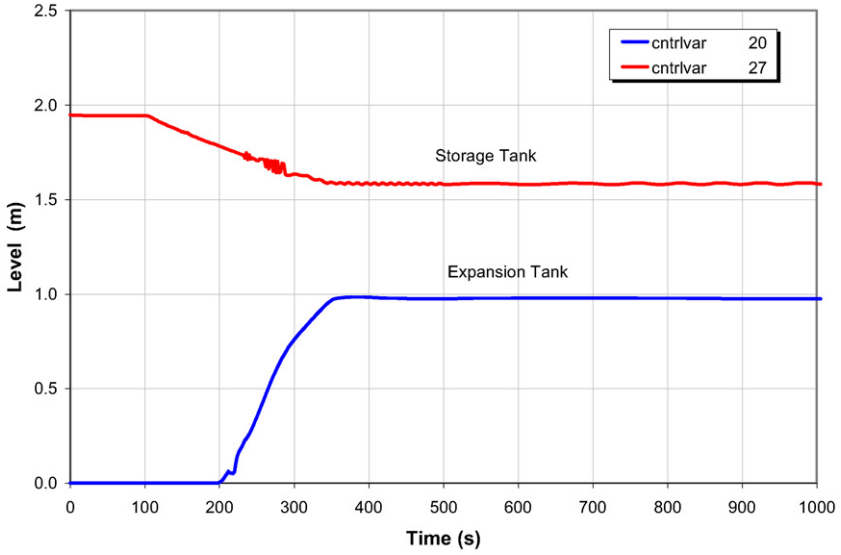

Fig. 6. Transient No. 1: Expansion and storage tank level (the initial phase).

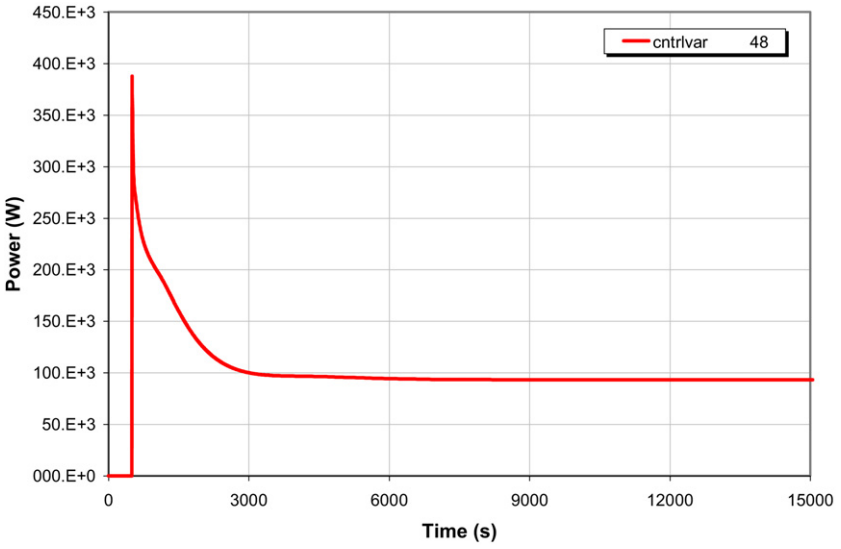

Fig. 7. Transient No. 1: Electric heater power.

at the second one. The atmosphere was simulated to account for the whole circuit heat losses to the environment.

6. PCS facility operational transient simulation

Three operational transients were simulated representing the main operating conditions of the PCS facility, in particular:

(1) Plant start-up and steady state without solar radiation;
(2) Solar radiation transient;
(3) Plant shut-down and circulation pump stop.

6.1. Transient No. 1

The initial conditions of this transient are a salt mixture level in the storage tank of 1.95 m as well as in the related inlet and outlet ducts, at 593.15 K temperature and 0.1 MPa pressure. All the rest of the circuit is full of air at atmospheric pressure with heat structures at 543.15 K. From these static conditions, the pump begins to circulate the salt mixture, filling-up the circuit and forming stable levels in the storage and expansion tanks with a steady state mass flow rate of 6.2 kg/s. When the circulation conditions are stable, the electric heater is switched-on and its outlet set point temperature is set at 603.15 K. The air cooler gates open when temperature at the second air cooler outlet reaches 588.15 K (set point 593.15 − 5 K) and natural circulation is established, while the fans start at 595.15 K (set point 593.15 + 2 K) and produce a forced flow. Steady conditions are reached with the electric heater compensating for heat losses to the environment and heat dissipated in the air coolers.

The salt mixture mass flow rate is shown in Fig. 5. It reaches a peak of 13.4 kg/s, then diminishes to a stable value of 6.2 kg/s as the circuit hydraulic resistance increases due to gradual fill-up of pipes that were initially full of air. Levels in the storage and expansion tanks are shown in Fig. 6. The electric heater power is shown in Fig. 7. Because the electric heater

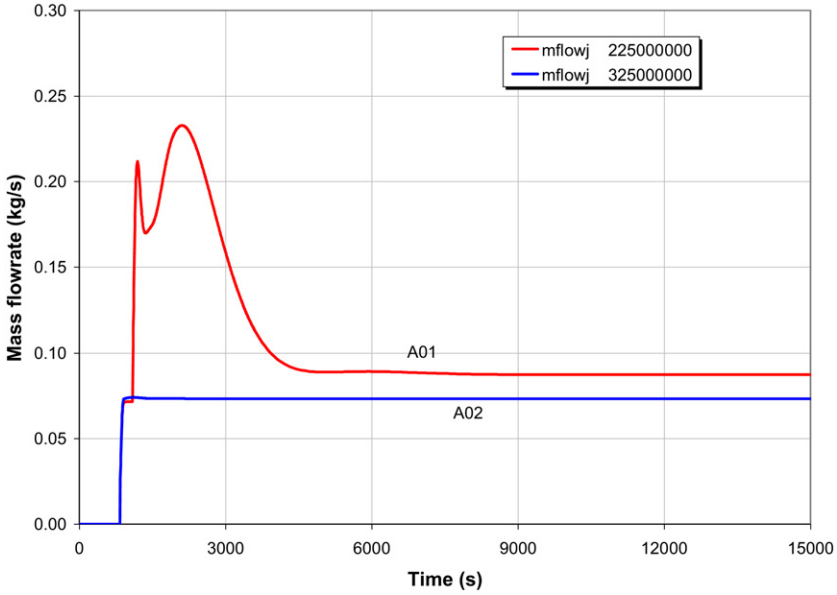

Fig. 8. Transient No. 1: Air cooler air mass flow rates.

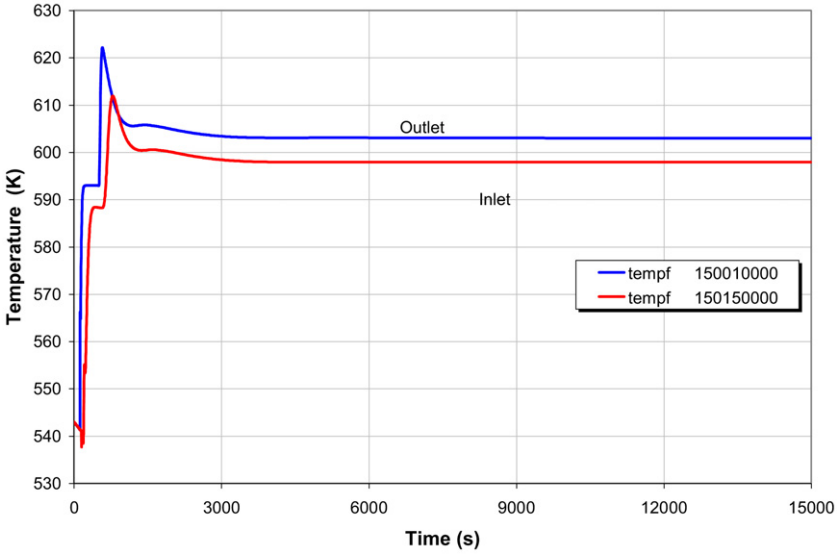

Fig. 9. Transient No. 1: Test section inlet and outlet temperatures.

is regulated on the basis of temperature error between heater outlet and set-point, an initial power peak is provided to compensate for the difference. The power is established at 93.2 kW. The air cooler mass flow rates are shown in Fig. 8 and they include both the natural and forced circulation. Air cooler A02 is in natural circulation because its fan starts only when the air cooler A01 fan is at its maximum mass flow rate. The respective steady air mass flow rates of 0.087 kg/s and 0.073 kg/s are sufficient to maintain the A02 outlet temperature at the set point value. The test section inlet and outlet temperatures are shown in Fig. 9. The largest heat losses occur in the test section that determine the 5 K temperature decrease, while 1 K is lost by insulated piping. No thermal stratification occurs in the storage tank, which stabilizes at 593 K.

The steady state conditions reached at the end of transient No. 1 are the initial conditions for transient No. 2.

6.2. *Transient No. 2*

The initial conditions of this transient are a salt mixture level in the storage tank of 1.59 m and of 0.97 m in the expansion tank, a constant fluid mass flow rate of 6.2 kg/s, an electric heater outlet temperature of 603.15 K, a second air cooler outlet temperature of 593.15 K, natural circulation of air in both the air coolers and a limited forced circulation of air in air cooler A01.

A curve of solar power to the test section is input to the code that reproduces the trend of solar radiation during the day. When the power curve goes to zero, after the daily excursion, the air cooler gates are closed and the electric heater compensates for the heat losses to the environment.

The power curve reproduces an experimentally recorded daily solar excursion and reaches a maximum of 317 kW, as

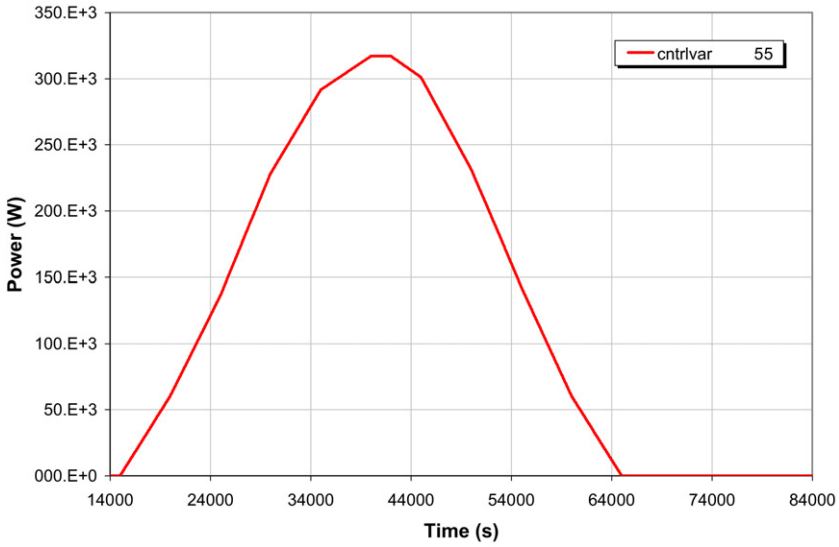

Fig. 10. Transient No. 2: Solar power.

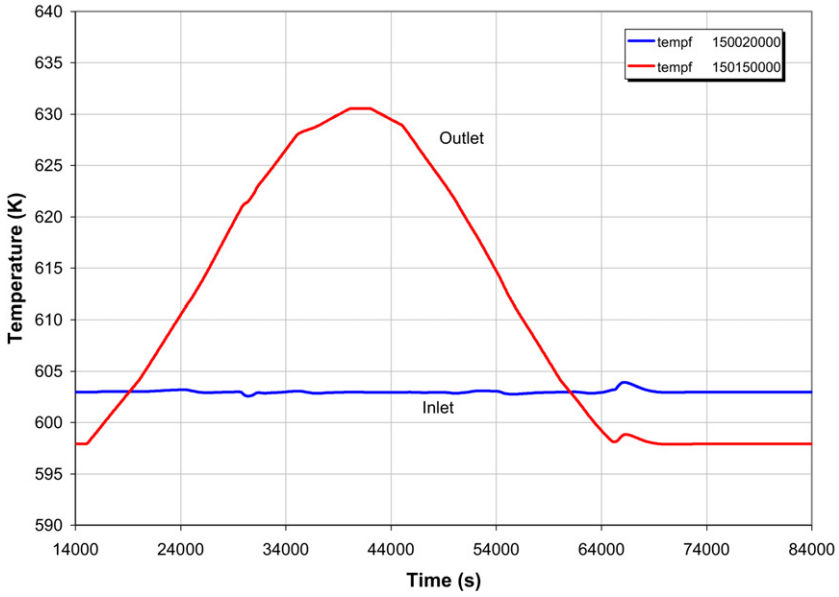

Fig. 11. Transient No. 2: Test section inlet and outlet temperatures.

shown in Fig. 10. The salt mixture temperature at the test section outlet follows the solar power trend and reaches a maximum of 630.5 K, while the inlet temperature is almost constant. The test section inlet and outlet temperatures are shown in Fig. 11. During the power excursion transient, the control system regulates the fan mass flow rates to maintain the air cooler A02 outlet temperature as close as possible to the set-point. The maximum temperature error from the set-point, calculated during the rising and decreasing phases of power, is less than 4 K and is smaller in the central phase of the transient, Fig. 12. The air cooler air mass flow rates are shown in Fig. 13. As a consequence of the test section heat-up, temperature increases at the air cooler inlet and the fan air mass flow rate increases at the first air cooler to compensate for the temperature error with respect to the set-point. When the first fan reaches the maximum mass flow rate of 7 kg/s, the second fan is started. Having the second fan being either on or off, its air mass flow rate is set to maximum and, in order to avoid discontinuities in the heat transfer, the first fan mass flow rate is reduced to zero and regulated from there. The heat transfer coefficient at the maximum air mass flow rate is estimated to be 23.2 $W/m^2 K$. At time 65000 s, solar power is zero and the air cooler gates are closed to avoid cooling the fluid. The electric heater power is regulated during the entire transient to maintain the outlet temperature at the set-point, as shown in Fig. 14. The total heat losses estimated corresponding to the maximum solar power are 66.1 kW. At the end of the transient, after the air cooler gate closure, the electric heater compensates for a heat loss of 57.5 kW. The steady conditions reached at the end of transient No. 2 are the initial conditions for transient No. 3.

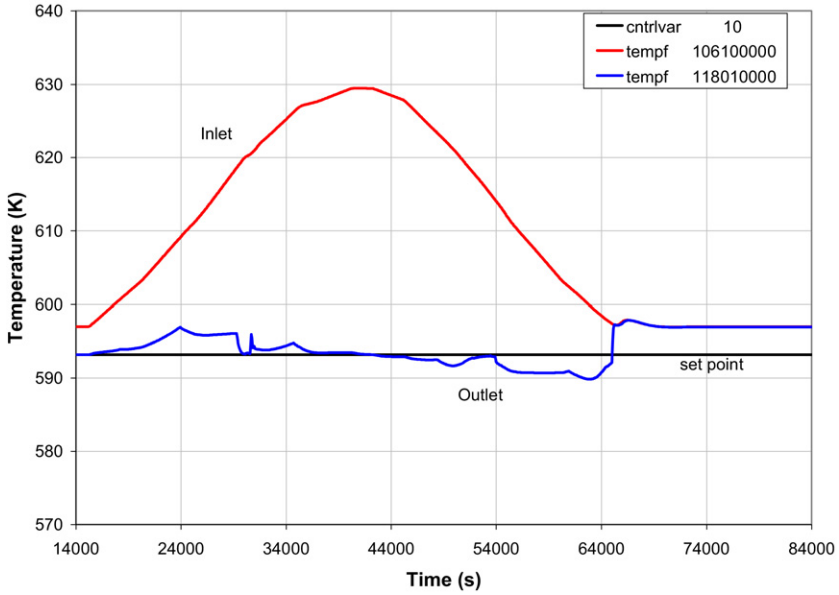

Fig. 12. Transient No. 2: Air cooler inlet and outlet temperatures.

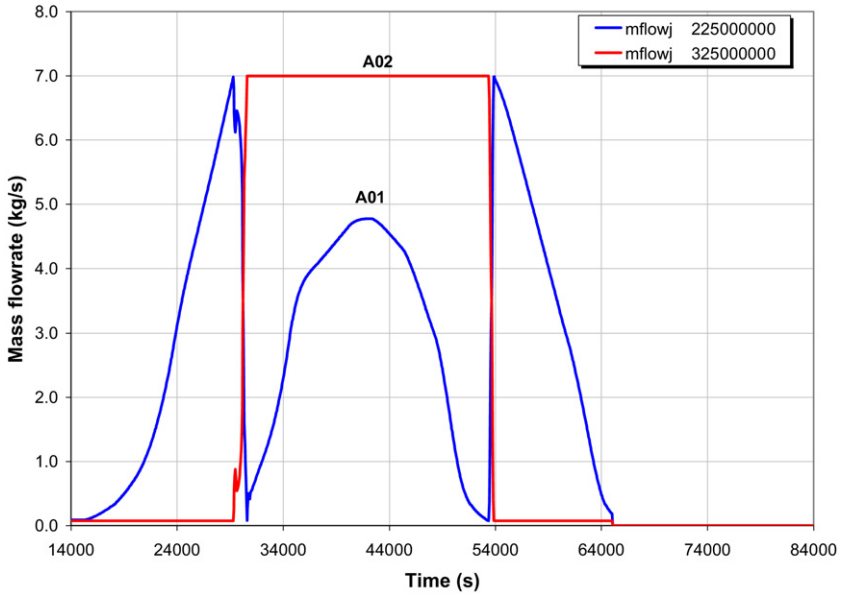

Fig. 13. Transient No. 2: Air cooler air mass flow rates.

6.3. *Transient No. 3*

The initial conditions of this transient are a salt mixture level in the storage tank of 1.59 m and of 0.99 m in the expansion tank, a constant fluid mass flow rate of 6.27 kg/s, and an electric heater power output of 57.2 kW to balance the heat losses to the environment. The absolute pressure in the circuit was risen from 0.1 to 0.199 MPa in order to avoid computer code run stoppage caused by the low salt steam partial pressure that is established in the expansion tank when it empties.

From these conditions a pump stop signal leads to a pump stop in 10 sec. Once the pump speed is zero, gravity drives the fluid contained in the circuit to the storage tank, which is the lowest point of the circuit. The mass flow rates in the two branches of the circuit (rising from storage tank to expansion tank and descending from expansion tank and storage tank) gradually reduce to zero, Fig. 15. The level in the expansion tank decreases just after the pump stops while the storage tank level increases as fluid contained in the two branches continues to pour off into it, Fig. 16.

At time 85914 sec, the calculation stopped due to a minimum fluid temperature error in one of the test section volumes. None of the attempts to restart the calculation was successful. Regardless, the transient trend was already defined with pipes emptying but with liquid still present in some areas.

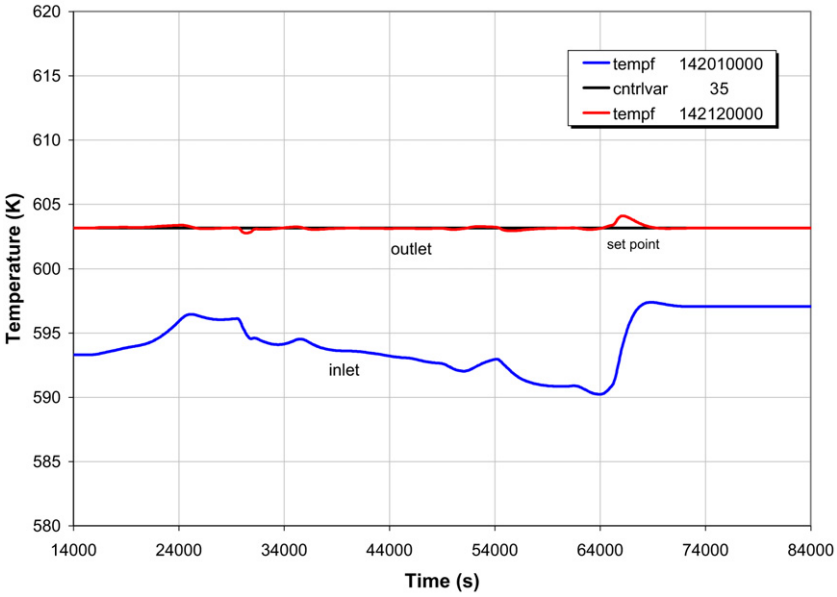

Fig. 14. Transient No. 2: Electric heater inlet and outlet temperatures.

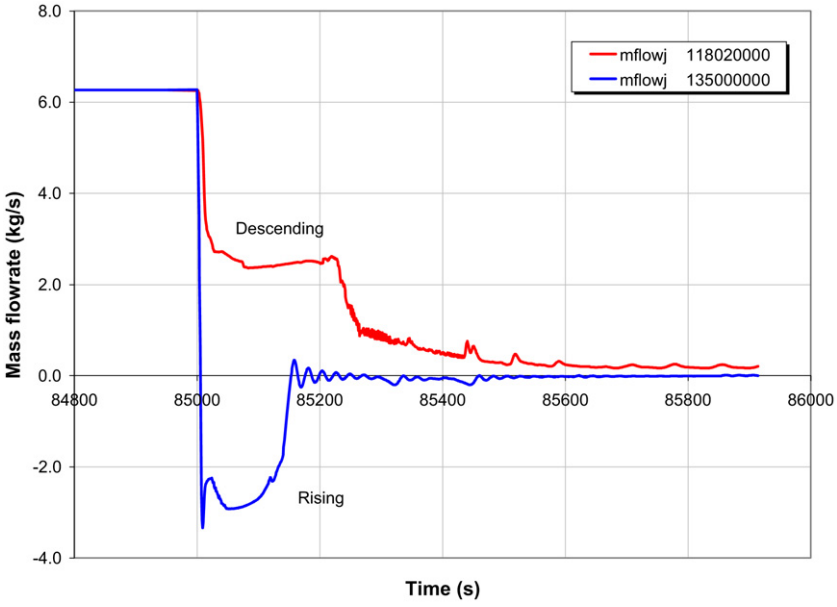

Fig. 15. Transient No. 3: Rising and descending branch mass flow rates.

7. Conclusions

Within the framework of a research activity on alternative energy sources, in particular within the thermodynamic solar design of ENEA, an instrument for numerical simulation of circuits containing a molten salt mixture (sodium and potassium nitrates) suitable for complex thermodynamic system behavior analyses was set-up in order to demonstrate the effectiveness of electric energy and high temperature heat production.

The RELAP5 Mod3.2.2 beta code was modified to introduce a new fluid consisting of a molten salt mixture of 60% $NaNO_3$ and 40% KNO_3 , which was validated versus experimental data of the PCS facility electric heater [13].

A complete numerical model of the PCS test facility, built at the ENEA Research Centre of Casaccia, was set-up for the modified RELAP5 code and two operational transients were simulated: a start-up transient and a solar power excursion during the day. An additional transient was simulated: a pump start-up and circuit emptying that provided indications on the utilization limits of the code [15].

Two important points were obtained by this research activity:

– The modified RELAP5 code can reproduce the main experimental phenomenology both from the dynamic and thermal point of view;

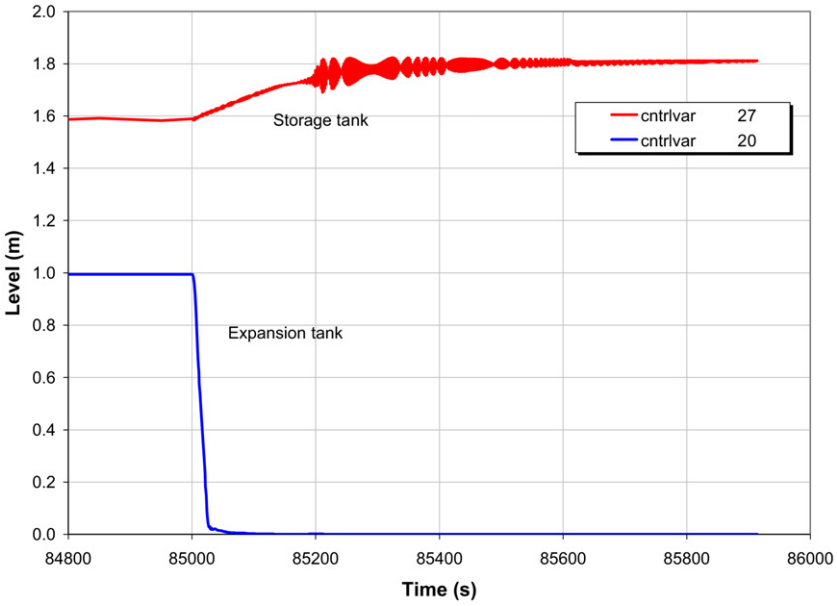

Fig. 16. Transient No. 3: Expansion and storage tank levels.

– A flexible analytical tool is available to be used to support the design and experimentation activities in the ENEA thermodynamic solar design.

Further validation of the RELAP5 code versus other experimental transients of the PCS facility would confirm once more the possibility of code utilization to simulate even more complex and larger power circuits.

Acknowledgements

The authors wish to thank Mr. Edward Dustin Schrull for his accurate review of the manuscript.

References

[1] U. Herrmann, B. Kelly, H. Price, Two-tank molten salt storage for parabolic trough solar power plants, Energy 29 (2004) 883–893.
[2] D. Kearney, B. Kelly, U. Herrmann, R. Cable, J. Pacheco, R. Mahoney, H. Price, D. Blake, P. Nava, N. Potrovitza, Engineering aspects of a molten salt heat transfer fluid in a trough solar field, Energy 29 (2004) 861–870.
[3] R. Tamme, Development of storage systems for SP plants, in: DG TREN-DG RTD Consultive Seminar "Concentrating Solar Power", Brussels, 27 June 2006, DLR German Aerospace Center, Institute of Thermodynamics, Stuttgart/Koln/Almeria.
[4] RELAP5/MOD3 code manual, NUREG/CR-5535, INEL-95/0174.
[5] A. Miliozzi, G.M. Giannuzzi, P. Tarquini, A. La Barbera, ENEA Progetto solare ad alta temperatura: Fluido termovettore: dati di base della miscela di nitrati di sodio e potassio, ENEA/SOL/RD/2001/07, Rev. 0.0.
[6] A.B. Zavoico, Solar power tower design basis document, Sandia National Laboratories, SAND 2001–2100, Rev. 0. Nexant, San Francisco, 94104 CA, July 2001.
[7] Perry's Chemical Engineers' Handbook, sixth ed., McGraw-Hill International Editions.
[8] E. Pedrocchi, M. Silvestri, Termodinamica tecnica, Terza edizione, Città Studi srl, 1995.
[9] V.I. Glazov, G.P. Dukhanin, K.K. Shrainer, Thermodynamic characteristics of the system $NaNO_3$–KNO_3, Russian Journal of Applied Chemistry 67 (7) (1994); Plenum Publishing Corporation 1995 (Part 1).
[10] V.I. Glazov, G.P. Dukhanin, Partial Pressure of Saturated Sodium Nitrate Vapor Above $NaNO_3$–KNO_3 System, Plenum Publishing Corporation, 1993.
[11] V.I. Glazov, P.S. Golovanov, G.P. Dukhanin, Saturated Vapor Pressure of the $NaNO_3$–KNO_3 System, Plenum Publishing Corporation, 1990.
[12] A.B. Zavoico, Solar Power Two. Design Basis Document, Sandia 2001–2100, July 2001.
[13] R. Ferri, A. Cammi, Implementazione delle proprietà dei sali fusi nel codice Relap5 e verifica della sua funzionalità, SIET 01 155 RT 04, Piacenza, 15 luglio 2004.
[14] Personal communication from Mazzei to Ferri, e-mail June 15, 2004.
[15] R. Ferri, Modellizzazione dell'impianto PCS ed esecuzione di calcoli di transitori operazionali con il codice Relap5, SIET 01 189 RT 04, Piacenza, 31 marzo 2005.